Magnetic cloud distortion resulting from propagation through a structured solar wind: Models and observations

JOURNAL OF GEOPHYSICAL RESEARCH, VOL. 111, A12109, doi:10.1029/2006JA011903, 2006

Magnetic cloud distortion resulting from propagation through a structured solar wind: Models and observations

M. J. Owens[1]

Received 7 June 2006; revised 15 September 2006; accepted 10 October 2006; published 20 December 2006.

[1] Numerical simulations of magnetic clouds (MCs) propagating through a structured solar wind suggest that MC-associated magnetic flux ropes are highly distorted by inhomogeneities in the ambient medium. In particular, a solar wind configuration of fast wind from high latitudes and slow wind at low latitudes, common at periods close to solar minimum, should distort the cross section of magnetic clouds into concave-outward structures. This phenomenon has been reported in observations of shock front orientations, but not in the body of magnetic clouds. In this study an analytical magnetic cloud model based upon a kinematically distorted flux rope is modified to simulate propagation through a structured medium. This new model is then used to identify specific time series signatures of the resulting concave-outward flux ropes. In situ observations of three well studied magnetic clouds are examined with comparison to the model, but the expected concave-outward signatures are not present. Indeed, the observations are better described by the convex-outward flux rope model. This may be due to a sharp latitudinal transition from fast to slow wind, resulting in a globally concave-outward flux rope, but with convex-outward signatures on a local scale.

Citation: Owens, M. J. (2006), Magnetic cloud distortion resulting from propagation through a structured solar wind: Models and observations, *J. Geophys. Res.*, *111*, A12109, doi:10.1029/2006JA011903.

1. Introduction

[2] Observations of coronal mass ejections (CMEs) and the resulting interplanetary CMEs (ICMEs) are generally limited to remote coronal observations and a single in situ spacecraft observation, respectively, though a limited number of multispacecraft in situ observations of an ICME have been reported [e.g., *Riley et al.*, 1997]. Thus modeling and simulation results of the evolution of ICMEs during their propagation through the heliosphere have been pivotal in understanding and interpreting the limited information available.

[3] Magnetic clouds (MCs) are a subset of ICMEs characterized primarily by a smooth rotation in the magnetic field direction and enhancement in the magnetic field intensity as the transient structure passes over an observing spacecraft [*Burlaga et al.*, 1981]. This signature has been interpreted and modeled as a force-free magnetic flux rope, enabling the global properties of MCs to be derived from single-point in situ measurements [e.g. *Burlaga*, 1988]. In reality, the flux rope is unlikely to be force-free, with deviations away from a circular cross section arising from both expansion in a spherical geometry [*Riley and Crooker*, 2004] and interaction with an inhomogeneous medium [e.g., *Riley et al.*, 1997; *Manchester et al.*, 2004].

[4] As CMEs typically have angular widths of $\sim 50-60^{\circ}$ and originate from latitudes close to the streamer belt [e.g., *Hundhausen*, 1993; *Gopalswamy*, 2004], they may frequently experience large gradients in ambient solar wind speed over their latitudinal extent. This effect will be particularly prevalent at times close to solar minimum, when high-speed solar wind typically emanates from the high latitude polar regions, and slower wind comes from the low latitude helmet streamer-associated regions [e.g., *McComas et al.*, 2003]. Numerical hydrodynamic simulations of CME-like density clouds propagating into such a bimodal medium suggest the cross-sectional shape of the transient structure becomes highly distorted [*Riley et al.*, 1997], resulting in a concave-outward shape if the center of the density cloud is close to the latitude of the solar wind speed minimum [*Odstrcil and Pizzo*, 1999]. This distortion has been shown to occur even when the magnetic flux rope structure of a magnetic cloud is included [*Odstrcil et al.*, 2004a; *Schmidt and Cargill*, 2001; *Manchester et al.*, 2004], as the flow momentum greatly exceeds any restraining forces arising from magnetic tension [*Riley and Crooker*, 2004].

[5] Observational evidence for this phenomenon has so far been limited to deformation of shock fronts ahead of ICMEs [*Burton et al.*, 1992], though data-driven shock propagation models also find evidence of decreased shock speeds close to the ambient solar wind speed minimum

[1]Center for Space Physics, Boston University, Boston, Massachusetts, USA.

0148-0227/06/2006JA011903$09.00

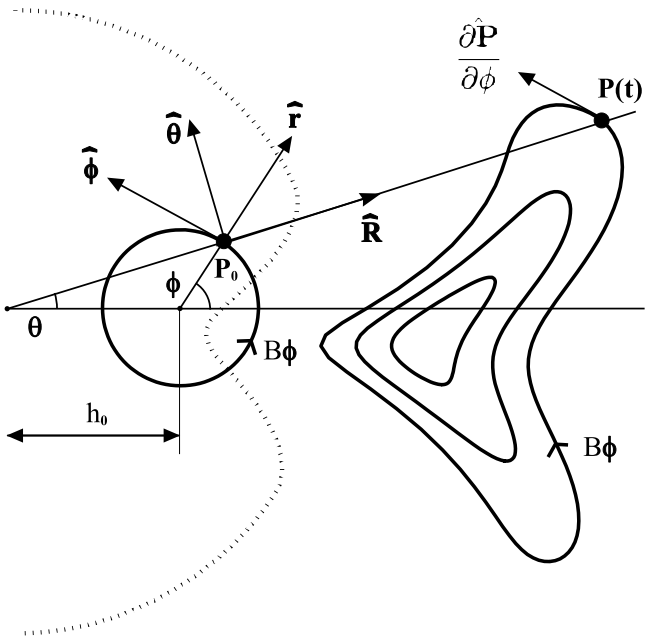

Figure 1. A schematic representation of the geometry used to generate the kinematically distorted flux rope model in a structured solar wind. A constant-α force-free flux rope is initially located at a heliocentric height h_0. Each point within the flux rope then moves subject to 2 velocities: antisunward (the $\hat{\mathbf{R}}$ direction) at speed $V_{TR}(\theta)$ and antiaxially (the $\hat{\mathbf{r}}$ direction) at a speed V_{EX}. The dashed line shows the $V_{TR}(\theta)$ profile. See also Figure 2.

[*Smith et al.*, 1996]. However, this effect has not been reported in the body of ICMEs (i.e., within the magnetic flux rope in the case of MCs). In this study an analytical magnetic cloud model based upon a kinematically-distorted flux rope [*Owens et al.*, 2006, hereinafter referred to as "Paper 1"] is modified to simulate propagation through a structured solar wind flow. This new model is then used to predict observable signatures of the resulting concave-outward flux rope structure. In situ observations of three well documented magnetic cloud encounters are analyzed for evidence of such signatures.

2. Flux Ropes in a Structured Solar Wind

[6] Recently, a model for the magnetic field structure of MCs has been developed that accounts for kinematic-distortion of the flux rope which naturally arises from internal pressure-driven expansion during antisunward propagation (Paper 1). This results in a flattened flux rope cross section, very similar to the concave-outward "pancake" structures obtained by numerical simulations of ICMEs in an approximately uniform solar wind [e.g. *Riley and Crooker*, 2004; *Riley et al.*, 2004].

[7] The analytical expression for the kinematically distorted flux rope model of Paper 1 is derived in the following manner (see Paper 1 for a more detailed description of the model): at time $t = 0$, the magnetic cloud is assumed to take the form of a constant-α, force-free flux rope of radius r_0, axial field strength B_0 and helicity H at a position $P_R = h_0$, $P_\theta = 0$ in heliocentric polar coordinates (see Figure 1). As in Paper 1 α, defined by $\mathbf{J} = \alpha\mathbf{B}$, $\mathbf{J}$ and $\mathbf{B}$ being the current density and magnetic field vectors, respectively, is set to 2.408. This defines the flux rope outer boundary to be the distance from the axis at which the field becomes completely poloidal field.

[8] Positions within the flux rope are described by flux rope axis-centered polar coordinates ($\hat{\mathbf{r}}$, $\hat{\phi}$), with $\phi = 0$ coinciding with $\theta = 0$. Each point within the flux-rope then moves subject to two velocities: expansion at speed $V_{EX}r/r_0$ in the $\hat{\mathbf{r}}$ direction and transit in the $\hat{\mathbf{R}}$ direction at speed V_{TR}. An expansion factor, A, is defined as the ratio of V_{EX} to V_{TR}. To maintain a constant angular extent, as is frequently reported in coronagraph observations of CMES [e.g., *Hundhausen*, 1993; *St. Cyr. et al.*, 2000; *Gopalswamy*, 2004], it is necessary to limit the expansion velocity to the $\hat{\mathbf{R}}$ component. Thus at a time t, a point initially inside the flux rope at a point $\mathbf{P_0} = (P_{R0}, P_{\theta 0})$ will be at:

$$\begin{aligned} P_R(t) &= P_{R0} + tV_{TR} + tV_{EX}\frac{r}{r_0}\cos(\phi - \theta) \\ P_\theta(t) &= P_{\theta 0} \end{aligned} \tag{1}$$

[9] In Paper 1, V_{TR} was assumed to be constant. In this study, a θ dependence is added to V_{TR} to simulate the flux rope's response to the latitudinal variation in solar wind speed. Thus it is assumed parts of the flux rope embedded in fast solar wind transit faster than parts of the flux rope in slower solar wind, in a process analogous to aerodynamic drag [*Cargill*, 2004]. This approach ignores magnetic tension forces in the flux rope that would act to resist distortion. Numerical MHD simulations of flux ropes treat the evolution of the magnetic fields self-consistently and suggest that even in the high beta regime of magnetic clouds this is a valid approximation, as the flow momentum is much greater than the restraining magnetic tension forces [*Schmidt and Cargill*, 2001; *Manchester et al.*, 2004]. However, we note that the model is probably less applicable to magnetic clouds with extremely strong magnetic fields.

[10] In principal any analytical or data derived function of $V_{TR}(\theta)$ could be used, so long as the function is continuous (to preserve $\nabla \cdot \mathbf{B} = 0$), positive and the minimum value of V_{TR} is greater than V_{EX} (so as to provide a physical solution). This study uses the following analytical form (see also Figure 2):

$$\begin{aligned} \left|\frac{\pi\theta}{\theta_W} - \theta_0\right| &\geq \pi; \qquad V_{TR} = V_{MAX} \\ \left|\frac{\pi\theta}{\theta_W} - \theta_0\right| &\leq \pi; \qquad V_{TR} = V_{MAX} - \frac{\Delta V}{2}\left[1 + \cos\left(\frac{\pi\theta}{\theta_W} - \theta_0\right)\right] \end{aligned} \tag{2}$$

where V_{MAX} is the transit speed of the fastest moving part of magnetic cloud, and the remaining parameters describe a sinusoidal dip in transit speed: ΔV is the depth of the dip (i.e., the maximum contrast between the fastest and slowest moving regions), θ_W is the width of dip and θ_0 determines the offset between the center of the dip and the flux rope axis. Thus with small values of θ_0, this equation approximates the effect on the magnetic cloud transit speed resulting from a solar wind speed configuration frequently found at solar minimum: fast wind emanating from the

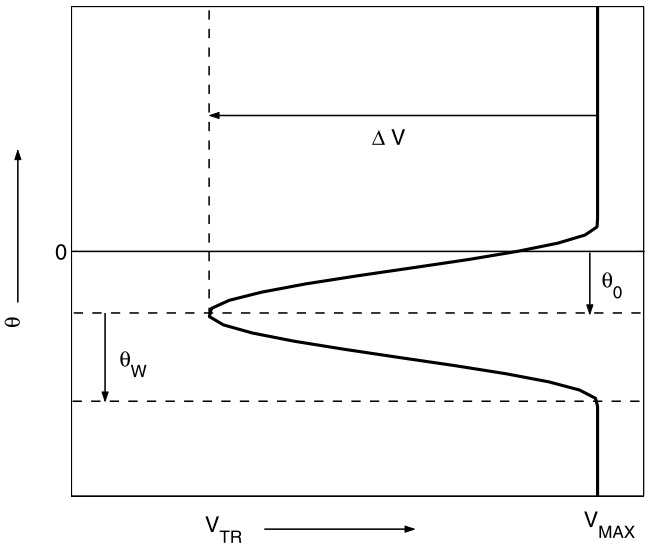

Figure 2. The latitudinally dependent form of the transit speed (V_{TR}) used in this study. There is a uniform transit speed of V_{MAX}, except for the sinusoidal dip at low latitudes (assuming θ_0 is small), characterized by a width (θ_W), depth (ΔV), and an offset relative to the flux rope axis (θ_0).

poles of the Sun, and slow streamer belt-associated wind at lower latitudes. Note that coronal and heliospheric models driven by the observed photospheric magnetic field [e.g., *Arge et al.*, 2004; *Odstrcil et al.*, 2004a, 2004b] frequently predict uniform fast wind at high latitudes with an approximately sinusoidal dip in solar wind speed associated with streamer belt latitudes. Thus it is assumed that V_{TR} varies in a similar manner to the ambient solar wind speed. The dashed line in Figure 1 shows the transit speed as a function of θ for V_{MAX} = 650 km/s, ΔV = 250 km/s, $\theta_W = \pi/6$ and $\theta_0 = \pi/9$. The right hand curves show the cross-sectional shape of the resulting magnetic cloud at 1 AU: a concave-outward shape is formed.

[11] As in Paper 1 it is assumed that for a given value of r, the ratio of axial to nonaxial magnetic field strengths is the same as in the force-free flux rope model. Thus only the cross-sectional shape of the constant-α force-free flux-rope is modified by the model, and the magnetic field structure is simply given by:

$$\begin{aligned}\mathbf{B}\left(\hat{\mathbf{R}},\hat{\boldsymbol{\theta}},\hat{\mathbf{Z}}\right) &= HB_0J_1(\alpha r)\frac{\partial\hat{\mathbf{P}}}{\partial\phi} + B_0J_0(\alpha r)\hat{\mathbf{Z}} \\ &= \left(HB_0J_1(\alpha r)\frac{\partial}{\partial\phi}[P_R(t)]\right)\hat{\mathbf{R}} \\ &\quad + \left(HB_0J_1(\alpha r)\frac{\partial}{\partial\phi}[P_\theta(t)]\right)\hat{\boldsymbol{\theta}} + B_0J_0(\alpha r)\hat{\mathbf{Z}} \\ &= HB_0J_1(\alpha r)\left(\frac{\partial P_{R0}}{\partial\phi} + tV_{EX}\frac{r}{r_0}\frac{\partial}{\partial\phi}\left[\cos(\phi-\theta)\right]\right. \\ &\quad \left. + t\frac{\partial V_{TR}}{\partial\phi}\right)\hat{\mathbf{R}} + HB_0J_1(\alpha r)\left(\frac{\partial P_{\theta 0}}{\partial\phi}\right)\hat{\boldsymbol{\theta}} \\ &\quad + B_0J_0(\alpha r)\hat{\mathbf{Z}} \\ \frac{\partial V_{TR}}{\partial\phi} &= \frac{\partial V_{TR}}{\partial\theta}\frac{\partial P_{\theta 0}}{\partial\phi}\end{aligned} \tag{3}$$

See Figure 1 and Paper 1 for more detail.

[12] This new form for the magnetic cloud magnetic field, used with a solar minimum-type solar wind speed configuration, gives concave-outward structures very similar to the morphology of the density perturbations at 1 AU described by [*Odstrcil et al.*, 2004b], and the concave-outward flux ropes of [*Manchester et al.*, 2004]. A magnetic field time series of an observing "spacecraft" is obtained by evolving this structure in time past a fixed point in space, as opposed to taking a radial cut through the structure at a fixed time (see Paper 1 for more detail). The next section outlines possible observable signatures of such concave-outward magnetic flux ropes.

3. Observational Signatures

[13] Convex-outward and concave-outward flux ropes, as produced by uniform and solar minimum-type solar wind configurations, respectively, result in markedly different in situ time series. Figure 3 shows the flux rope cross sections for a convex- (top) and concave-outward flux ropes (bottom) for the same flux rope parameters (listed in figure). The structured solar wind used to derive the concave-outward flux rope is parameterized by V_{MAX} = 650 km/s, with a speed dip fixed a the axis of the flux rope (i.e., $\theta_0 = 0$). The width of the dip is set to be equal to the angular width of the flux rope (i.e., $\theta_W = \pi/6$) so that there is some latitudinal speed gradient over the whole flux rope, as parts of the flux rope that extend out into uniform wind simply behave in an identical manner to the uniform solar wind flux rope of Paper 1. The depth of the dip (ΔV) determines how distorted the flux rope becomes by 1 AU. We choose a modest value of 250 km/s. Thus $V_{TR} = 650 - 125(1\cos[6\theta])$.

[14] The flux rope axis (Y', out of the page in Figure 3) is perpendicular to the radial direction. In geocentric solar ecliptic coordinates (GSE), the radial direction is $-X_{GSE}$ at the point of observation. The direction Z' is defined to be perpendicular to X_{GSE}, pointing north relative to the ecliptic plane (i.e., along Z_{GSE} when $Y' = Y_{GSE}$). The panels on the right show the magnetic field time series for a spacecraft intersecting the flux rope with an impact parameter of Y = 0.3, which is equivalent to 30% of the angular distance from the axis to the outer edge. The axial magnetic field variation ($B_{Y'}$) is very similar for both the convex- and concave-outward flux ropes. Note, however, that the axial field peaks sooner for the concave case because the low-latitude portion of the flux rope is transiting at a slower speed than in the convex case. Thus the expansion factor, A, is higher for the concave flux rope due to the dip in V_{TR}.

[15] The overall form of $B_{Z'}$ is also reasonably similar between the convex and concave cases, though it is consistently lower in magnitude for the concave case. The major difference occurs in B_{XGSE}. For the convex case, B_{XGSE} is small compared to the other components, and remains positive throughout the flux rope crossing, peaking at the center. However, for the concave case, B_{XGSE} is large and displays a bipolar variation, passing through zero at the center. The variation in the two nonaxial magnetic field components (B_{XGSE} and $B_{Z'}$) can be summarized by considering the angle, γ, between the magnetic field vector in the nonaxial ($X_{GSE}Z'$) plane and the Z' direction, measured through positive X_{GSE} (see Figure 3). For the convex-outward flux rope, γ remains positive throughout the

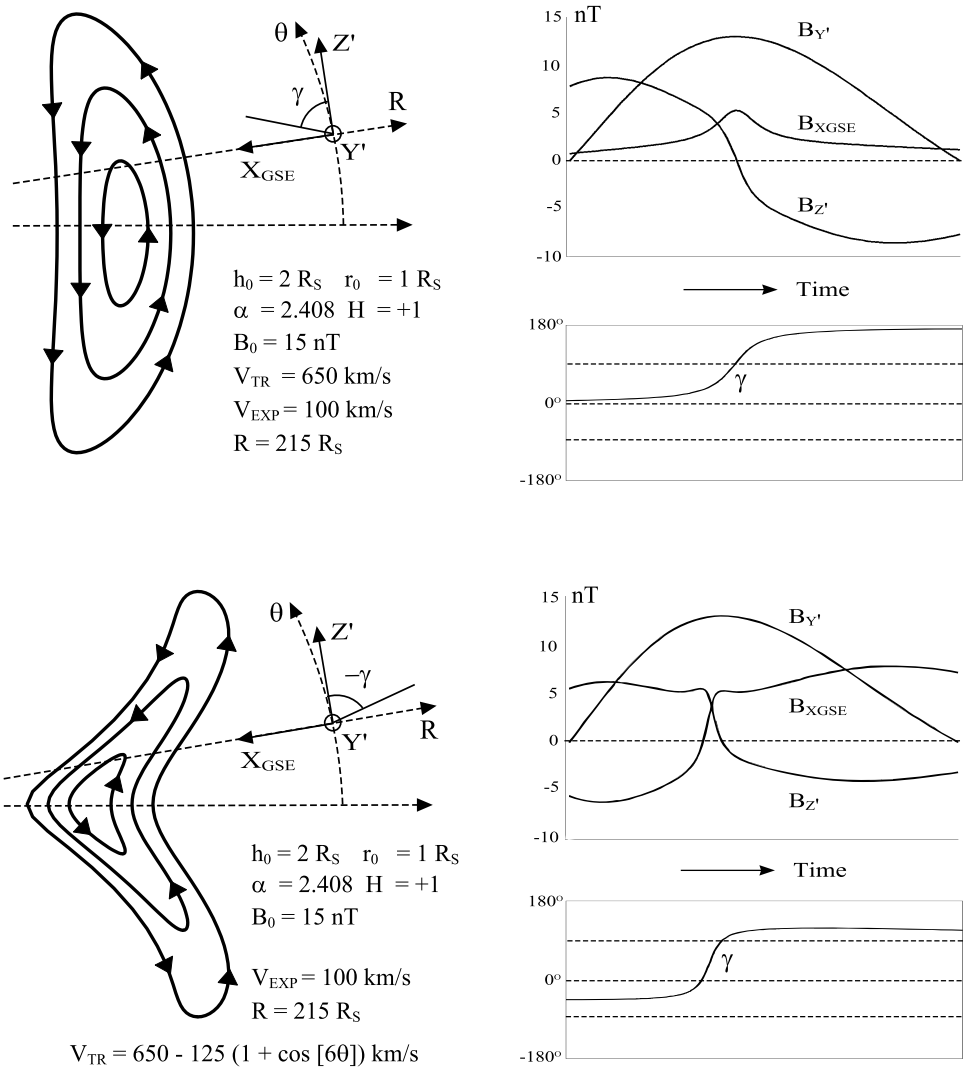

Figure 3. The cross sectional morphology and associated time series for convex- (top) and concave-outward (bottom) flux ropes. The flux rope axes lie along Y' (out of page). Here γ is defined as the angle between the flux rope magnetic field vector and the Z' direction, measured through positive X_{GSE}. The time series of γ show markedly different behaviors for convex and concave flux ropes.

spacecraft encounter, whereas for the concave-outward flux rope, γ displays a bipolar signature.

[16] Figure 4 shows the predicted γ profiles for spacecraft impact parameters (Y_0) of 0.9, 0.6, 0.3, 0.01, −0.3, −0.6 and 0.9 and for flux rope expansion speeds (V_{EX}) of 10, 50, 100, 150, 200, 250 km/s. In all cases $H = +1$, $\alpha = 2.408$, $r_0 = 1R_S$, $h_0 = 2R_S$ and $V_{TR} = 650$ km/s. The left hand plots are for the convex-outward flux rope, whereas the right hand plots use a structured solar wind with $V_{MAX} = 650$ km/s, $\Delta V = 250$ km/s, $\theta_0 = 0$ and $\theta_W = \pi/6$ to give a concave-outward flux rope, as per Figure 3. The resulting flux rope cross sections at 1 AU for the range of V_{EX} considered are shown below the γ time series plots. The γ plot limits are +180° to −180°, with the dashed line showing $\gamma = 0°$. The major difference between the convex- and concave-outward flux ropes is the polarity of γ: for the convex case, γ is always either completely positive or completely negative. However, for the concave case, γ always crosses through zero (except for very high $|Y_0|$ parameters: it is unlikely such "glancing" encounters would result in the identification of a magnetic cloud in in situ data). Note that for $Y_0 = 0$, there is no latitudinal speed gradient even for the concave case, hence the convex- and concave-outward flux rope time series are identical at this point. However, the 180° variation occurs earlier in the time series of the concave case because of the higher effective expansion speed.

4. Comparisons With Observations

[17] To maximize the possibility of finding the concave-outward flux rope signature in magnetic cloud observations, the events to which the model is compared must be carefully selected. The ambient solar wind needs to be essentially bimodal with latitude, limiting the time period from which events can be taken to the last solar minimum.

[18] As the model used to identify the concave-outward signature is essentially two-dimensional, it is necessary to select MC observations for which this is a reasonable

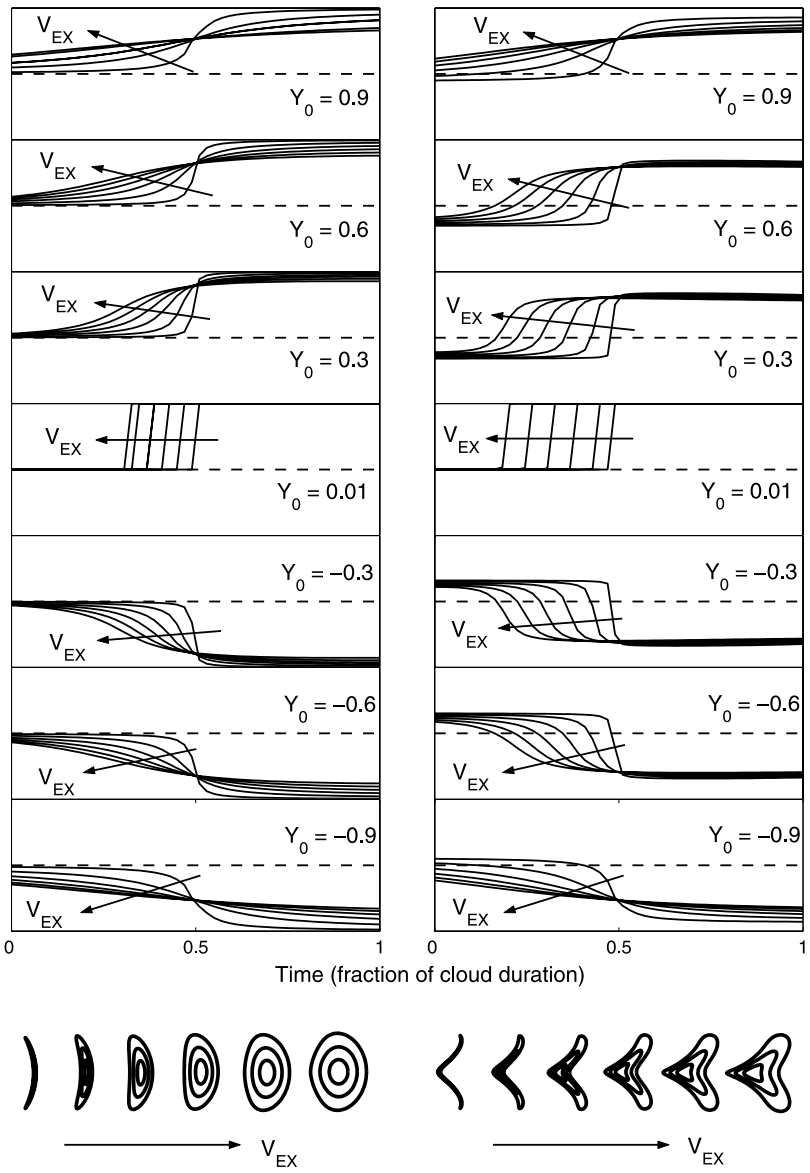

Figure 4. The predicted γ profiles for various spacecraft impact parameters (Y_0, the normalized distance of the closest approach of the spacecraft to the axis) and flux rope expansion speeds (V_{EX}). The plot limits are +180° to −180°, with the dashed line showing $\gamma = 0°$. Left (right) hand plots show the convex- (concave-) outward flux rope. The resulting flux rope cross sections at 1 AU are shown below the plots for the range of V_{EX} considered (10, 50, 100, 150, 200, and 250 km/s).

approximation. Hence the observed flux rope axis is required to be almost perpendicular to the radial direction, minimizing effects of axial curvature. This situation arises when a magnetic cloud is intercepted close to leading edge, or "nose," of the ejecta. It is often assumed that nose encounters arise when a magnetic cloud is associated with a full halo CME and activity close to the solar disc, as the CME velocity vector appears to be close to the Earth-Sun line. However, it should be noted that some apparently front-side halos CMEs do not result in ejecta at Earth [*Cane and Richardson*, 2003]. Additionally, for a concave-outward flux rope to be produced, the axis must be perpendicular to the direction of the solar wind speed variation. At solar minimum, when the speed variation is expected to be predominantly in the latitudinal direction, this translates to requiring the axis to lie close to the ecliptic plane. Combining these two axis orientation constraints means this study is limited to magnetic clouds with axes close to the $\pm Y_{GSE}$ direction.

[19] In this study we choose not to perform formal "fits" of the model to the data (e.g., by minimizing the mean-square-error between the model and observed magnetic field time series), as the aim of this study is to look for qualitative evidence of concave-outward flux ropes. As both the concave- and convex-outward flux rope models cannot both be representative of the true magnetic cloud structure, minimization of the model time series to match observations can be extremely misleading. Instead, we fix h_0, r_0, R, α and V_{TR} at default values (2 R_S, 1 R_S, 215 R_S, 2.408 and 650 km/s, respectively). Variation of these parameters does not greatly

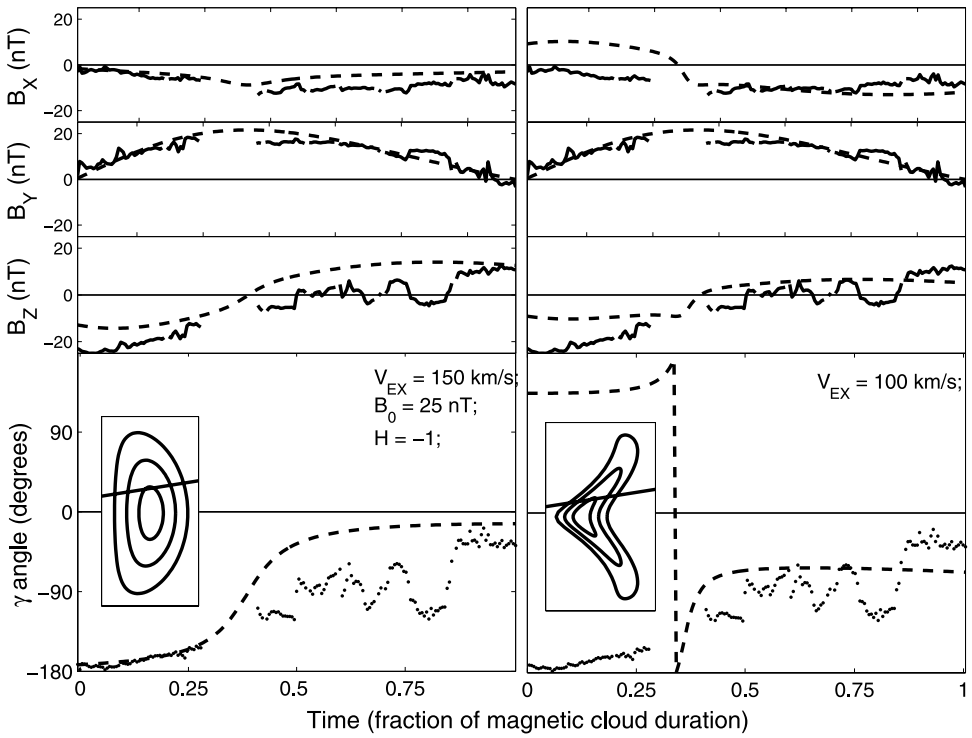

Figure 5. The 12 May 1997 halo CME resulted in this magnetic cloud on 15 May. Left (right) hand figures are for the convex- (concave-) outward flux rope model. The solid (dashed) lines in the top three panels show the three components of the observed (model) magnetic field in GSE coordinates. The bottom panel shows the time series of the γ angle. Inset is the cross section of the model flux rope when first encountered by the spacecraft, with Y_{GSE} pointing out of the page.

affect the resulting magnetic field time series. We choose to fix the impact parameter, Y_0, at a value of 0.3 (-0.3) for above (below) axis encounters. This value is large enough to differentiate between the convex and concave flux ropes, which are identical as $Y_0 \rightarrow 0$, but small enough to avoid classification as a "glancing encounter." Again, the value of this parameter (within reasonable limits) does not qualitatively change the resulting time series of γ: see Figure 4. The expansion speed, V_{EX} is determined by inspection of the asymmetry in the axial field time series, while the axial field strength, B_0, is set so as to match the magnitude of the magnetic field components: it does not vary the form of the field variation. The helicity of the flux rope (H) can be simply determined by inspection of the observed B_Z time series.

[20] To simulate a cloud propagating into a structured solar wind, we use V_{TR} with a θ dependence of the form outlined in equation (2). As in Figure 3, we set V_{MAX} = 650 km/s, $\theta_0 = 0$, $\theta_W = \pi/6$ and ΔV = 250 km/s, as these give concave-outward structures qualitatively similar to *Odstrcil et al.* [2004b] and *Manchester et al.* [2004].

4.1. Event of 15 May 1997

[21] The well studied CME of 12 May 1997 and resultant magnetic cloud at 1 AU on 15 May fit the event selection criteria very well. Both the semiemprical Wang-Sheeley-Arge (WSA) [*Arge et al.*, 2003] model and the MHD around a sphere (MAS) [*Linker et al.*, 1999] coronal MHD model use the observed photospheric magnetic field to derive a global solution to the ambient solar wind speed, and both predict the classic solar minimum bimodal solar wind structure at this time [*Arge et al.*, 2004; *Odstrcil et al.*, 2004b]. *Webb et al.* [2000] reported the CME formed a full, symmetric halo, with associated activity very close to the center of the solar disc. The resulting flux rope at 1 AU was determined to be almost exactly perpendicular to the radial direction (the axis was determined to lie along the Y_{GSE} direction). [*Odstrcil et al.*, 2004b] fit a cone model [*Zhao et al.*, 2002] to the coronagraph observations of the halo CME and determined the velocity vector to be within a few degrees of the Earth-Sun line. A density pulse with the same characteristics as the observed halo CME was injected into a numerical magnetohydrodynamic simulation of the heliosphere, using the MAS prediction of the ambient solar wind speed: the transient pulse became distorted into a concave-outward structure by 1 AU. In this section we look for similar distortion in the in situ measurements of the magnetic cloud flux rope.

[22] The thick solid lines in the top three panels of Figure 5 show the time series of the 5-min averaged magnetic field components (in GSE coordinates) observed by the MFI experiment on board the Wind spacecraft [*Lepping et al.*, 1995] within the magnetic cloud boundaries determined by *Webb et al.* [2000]. The classic unipolar variation in B_Y, starting and returning to zero, is characteristic of the axial field variation, meaning no transformation of the in situ data into flux rope coordinates of Figure 3 is necessary (i.e., $B_{XGSE} = B_X$, $B_{YGSE} = B_Y$ and $B_{ZGSE} = B_Z$). The slight asymmetry in the B_Y profile, with a peak just before half the cloud's duration suggests moderate expansion relative

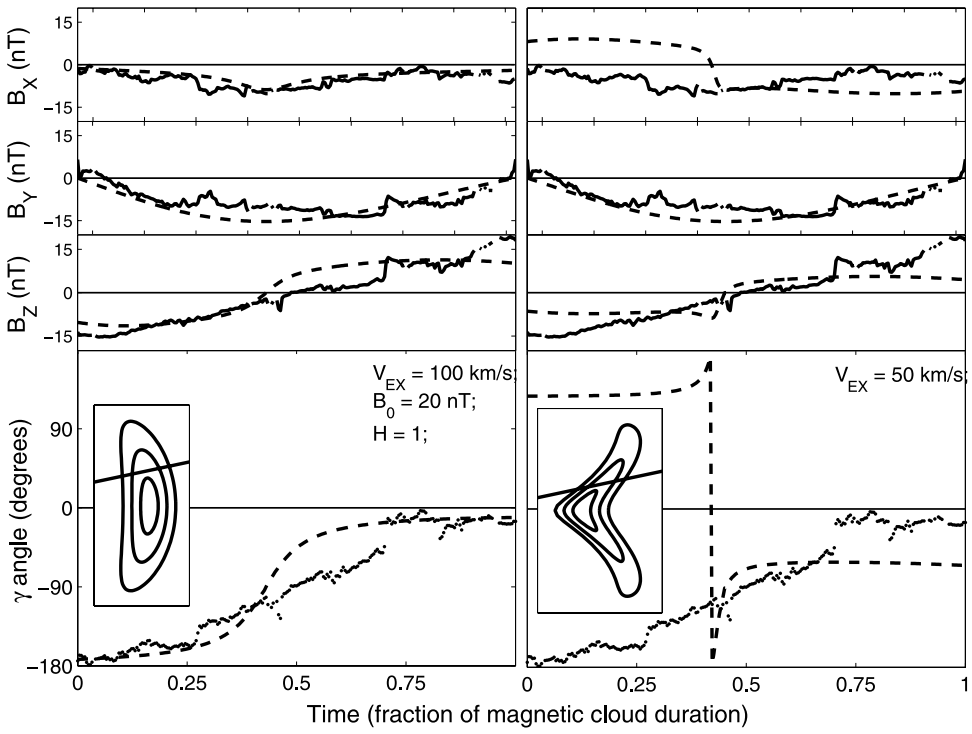

Figure 6. The 6 January 1997 halo CME resulted in this magnetic cloud on 10 January. Same format as Figure 5.

to its transit speed. The B_Z variation from negative to positive values is a clear indication of left-handed rotation of the magnetic field about the flux rope axis (i.e., $H = -1$). The persistently negative offset to B_X suggests that the spacecraft was below the axis relative to the ecliptic plane [e.g., *Owens and Cargill* 2004].

[23] On the basis of observed magnetic field components we set $H = -1$, $V_{EX} = 150$ km/s and $B_0 = 25$ nT (the helicity is the same as that of *Webb et al.* [2000], while the axial field strength is comparable to their estimate of 23 nT). The cross-sectional shape and point of interception is inset to the bottom left panel, with the Y_{GSE} direction pointing out of the page. The time series resulting from this convex flux rope model is shown as the dashed lines in the three top left panels: there is good agreement between all three components of the observed and modeled magnetic field components. The bottom left panel shows the observed (solid) and model (dashed) γ angle for the magnetic cloud. There is general agreement, particularly in the value of γ near the start and end of the cloud passage. Note that the model underestimates the inclination of the magnetic field to the Z direction between $\sim$0.4–0.8 of the cloud's duration.

[24] A concave-outward flux rope is obtained using the θ-dependent form of V_{TR}. Note that as this modified form of V_{TR} reduces the transit speed, it is necessary to reduce the expansion speed too: $V_{EX} = 100$ km/s matches the B_Y profile well. The resulting concave flux rope cross section and point of interception is inset to the bottom right figure. The dashed lines in the top right three panels of Figure 5 show the magnetic field time series in GSE coordinates. The variation in B_X and B_Z is summarized by the time series of γ (bottom right panel). The concave-outward model predicts γ should switch sign, from positive to negative, as the cloud passes over the observing spacecraft. This is not observed.

[25] Note that if the point of interception (Y_0) is varied so as to allow the best match between the concave flux rope model and observed magnetic field time series, $Y_0 \rightarrow 0$, which corresponds to no speed gradient, and the magnetic field configuration becomes the same as the convex case.

4.2. Event of 12 January 1997

[26] The second event we consider is the 6 January 1997 CME and resultant magnetic cloud on 10 January, which was well studied by [*Burlaga et al.*, 1998] due to the occurrence of the prominence-like material at the trailing end of the cloud. WSA and MAS coronal models both predict a bimodel solar wind structure at this time (N. Arge and P. Riley, personal communication, 2006. See also http://iMHD.net/mhdweb). This event has a full halo CME with transit vector determined to be very close to the Earth-Sun line [*Michalek et al.*, 2003]. As with the 12 May event, the axis of the associated magnetic cloud seems to be highly perpendicular to the radial direction: by inspection the axial field appears to lie along $-Y_{GSE}$. The profile of B_Y is fairly symmetric, suggesting less expansion than in the May 12th case. The negative to positive rotation of B_Z indicates a right-handed rotation about the axial field, and the negative offset to B_X suggests the spacecraft passed below the axis relative to the ecliptic [e.g., *Owens and Cargill*, 2004]. Thus we set $H = 1$, $V_{EX} = 100$ km/s and $B_0 = 20$ nT. Figure 6 shows the model and observed magnetic field components and γ angle (in the same format as Figure 5). Note the profile of γ is well matched for the convex case, though again there is an underestimation of the field inclination to the Z direction from about 0.4 to 0.7 of the cloud's duration.

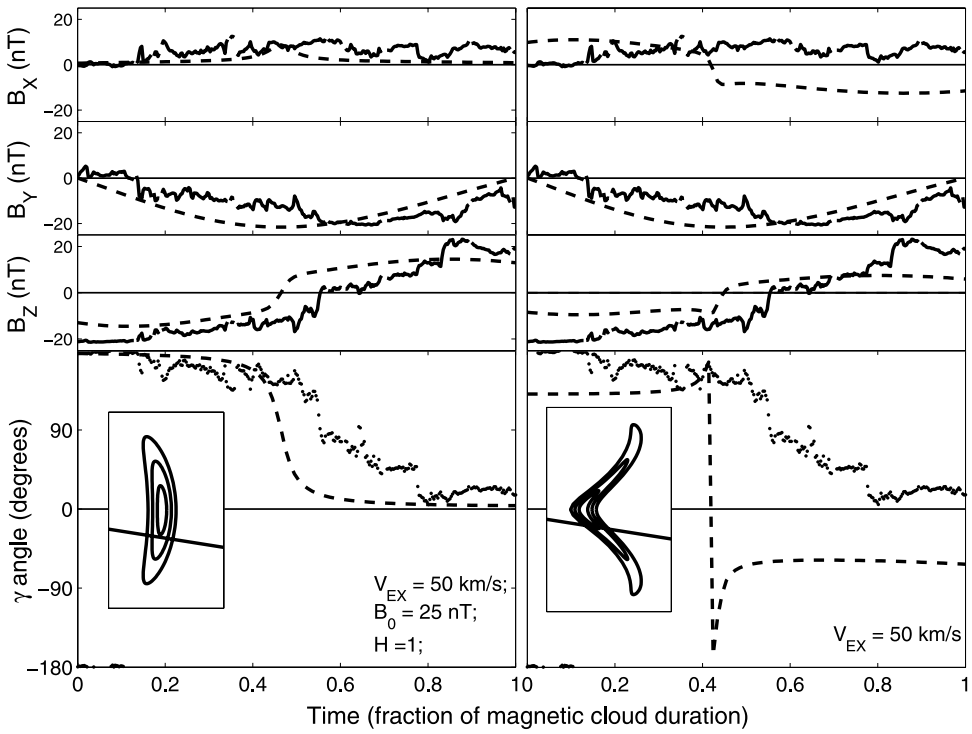

Figure 7. The magnetic cloud of 18 October 1995. Same format as Figure 5.

[27] To generate the structured solar wind flux rope model it is again necessary to reduce V_{EX} to account for the reduction of V_{TR} (V_{EX} = 50 km/s is used). Again, the bipolar variation of γ indicative of a concave-outward flux-rope does not seem to be present in the observations.

4.3. Event of 18 October 1995

[28] The final event considered is the magnetic cloud of 18 October 1995, which was studied extensively by *Lepping et al.* [1997]. Again, both WSA and MAS coronal models predict a bimodel solar wind structure at this time (N. Arge and P. Riley, personal communication, 2006. See also http://iMHD.net/mhdweb). Although there are no coronagraph observations at this time, *Lepping et al.* [1997] determined the axis of the magnetic cloud was very close to the Y_{GSE} direction, making it suitable for this study. Indeed, we find the unipolar variation in B_Y agrees with axial field pointing close to the $-Y_{GSE}$ direction. Figure 7 shows the the summary plot of the 18 October 1995 magnetic cloud (in the same format as Figure 5). As with the previous two events, the γ profile is much better matched by the convex-outward than the concave-outward model. Note also the underestimation of γ approximately halfway through the cloud.

5. Discussion

[29] In this study an existing magnetic cloud model based upon kinematically distorted flux ropes (Paper 1) was modified to include the effect of a structured solar wind, so as to give concave-outward structures thought to result from propagation into a solar minimum solar wind configuration. A robust signature of this concave-outward morphology was identified, and searched for in the spacecraft data. Three magnetic clouds were selected for their applicability to the analysis method and for their likelihood of forming concave-outward structures, due to both timing within the solar cycle and launch position. However, in all three cases the expected concave-outward signatures are not present. Furthermore, the simple uniform solar wind speed model, which forms convex-outward structures, fits the observations well. Possible causes of this surprising result can be broadly grouped into two categories: (1) the analysis methods used are not valid, and thus fail to detect the signatures of a concave-outward flux rope, and (2) the signatures of a concave-outward flux rope are not present in the in situ data (though the flux ropes may still be concave-outward on a global scale, as will be discussed).

[30] The first category is that where the analysis methods used are not valid.

[31] 1. The flux rope axis is not correctly determined for the in situ observations. This seems unlikely as the field in the determined axial direction matches very well what we expect from the model (along with the good fit of the model in general). Furthermore, for two of the three events, coronagraph and EIT observations suggest the magnetic clouds should be intercepted very close to the nose, and hence have axes perpendicular to the radial direction.

[32] 2. Effects of axial curvature are important and overwhelm the signatures we are looking for. For the apparent nose crossings selected for examination in this study, we expect the changes along the axial direction to be small compared to the changes perpendicular to the axis, and therefore the effect of curvature to be small.

[33] 3. Compression/rarefaction forces acting on the flux rope are not adequately taken into account, beyond the added latitudinal dependence of the local transit speed. While this would certainly change the magnetic field

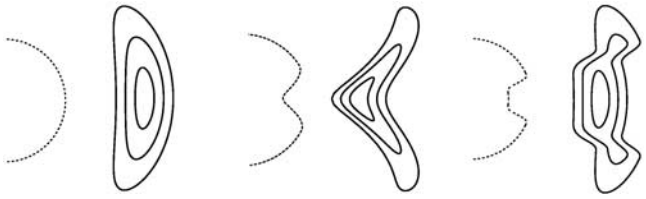

Figure 8. The flux rope cross sections (solid lines) resulting from different speeds as functions of latitudes (dashed lines). The left panel shows the uniform solar wind case, resulting in a convex-outward structure. The center panel shows a smooth dip in speed near the axis of the flux rope, which leads to the concave-outward cross section. The right panel shows a similar dip in speed close to the axis, but with a sharper transition from fast to slow wind. This results in a concave-outward structure on the global scale, but local in situ observations would reveal a convex-outward configuration of the flux rope field.

strength (this effect does seem to be observed by the underestimation of γ from 0.4 to 0.7 of the way through the MC crossing), it seems unlikely that this would have such a large effect on the magnetic field orientation throughout the flux-rope. However, it should be noted that two of the three magnetic clouds were followed by fast solar wind streams [*Odstrcil et al.*, 2004b; *Burlaga et al.*, 1998].

[34] The second category is that where signatures of concave-outward flux rope are not present in the data:

[35] 1. Magnetic cloud distortion by a structured solar wind simply does not occur: magnetic clouds largely ignore the effect of a bimodal solar speed as the magnetic tension resists distortion. This strongly contradicts the results of multiple numerical simulations. It would suggest that magnetic tension forces are being severely underestimated. This effect would be more pronounced in magnetic clouds with very strong magnetic fields.

[36] 2. The speed variation at low latitudes required to provide the distortion is not present (i.e., the real solar wind speed is approximately uniform with latitude). Highly unlikely, as both WSA and MAS models of corona at this time suggest the corona was ordered so as to produce slow wind at low latitudes and fast wind from poles, which agrees well with observations at 1 AU.

[37] 3. All three magnetic cloud encounters were made at precisely the latitude of the solar wind speed minimum, and hence had no latitudinal speed gradient. This is statistically unlikely, and the fact that the observed radial fields are non-zero suggest this is not the case.

[38] 4. Distortion is not present in single spacecraft in situ data because the transition from fast to slow wind is sharp, allowing the parts of the flux rope in fast/slow wind to expand independently [e.g., *Riley et al.*, 1997]. Discussed below.

[39] The left (center) panel of Figure 8 shows the cross sectional shape of a flux rope propagating through a uniform (structured) solar wind, resulting in a convex-(concave-) outward flux rope. The right panel shows a similar speed dip near the flux rope axis, but with a sharp latitudinal transition in speed. This results in the flux rope effectively breaking into separate latitudinal sections, which individually expand as per the uniform solar wind case. This would allow the flux rope structure to be concave-outward on a global scale, and thus drive shocks with a concave outward shape [*Burton et al.*, 1992; *Smith et al.*, 1996], but be convex-outward on a local scale, as measured by in situ observations.

[40] Further observational work is required to fully resolve this issue. In particular, multi-spacecraft observations of the same magnetic cloud, particular those well separated in latitude, will be necessary [e.g., *Riley et al.*, 1997; *Mulligan and Russell*, 2001]. Recent data from the solar mass ejection imager (SMEI) [*Jackson et al.*, 2004b] may be able to provide a unique insight into the global morpholgy of ICMEs, particularly in conjunction with tomographic techniques [*Jackson et al.*, 2004a]. A combined modeling/observation approach will also be useful: cone model fits to coronagraph images of halo CMEs [e.g., *Zhao et al.*, 2002; *Michalek et al.*, 2003] can provide an estimate of the velocity, position and width of a magnetic cloud, whereas coronal/heliospheric models such as WSA [*Arge et al.*, 2004] and MAS-ENLIL [*Odstrcil et al.*, 2004a] can provide a reconstruction of the ambient solar wind speed into which the clouds propagate. A parameterised relation between the solar wind speed and the local magnetic cloud transit speed may be possible [e.g., *Cargill* 2004].

[41] Finally, for the three events studied here, we note the overestimation of the flux rope magnetic field vector to the radial direction close to the middle/rear portion of the magnetic cloud. This suggests that this portion of the cloud is not as elongated as the kinematic flux rope model suggests. Three possible explanations present themselves: (1) that the constant α approach taken here needs to be modified, (2) ignoring magnetic forces is not a valid assumption in this region, (3) that rarefaction/compression effects need to be taken into account. A statistical study of a large number of magnetic clouds is required.

[42] **Acknowledgments.** This research was supported by the National Science Foundation under Agreement ATM-012950, which funds the CISM project of the STC program. We have benefited from the availability of Wind MFI data (P.I. R. Lepping). M.O. thanks Ying Liu of MIT for useful discussions.

[43] Zuyin Pu thanks David Webb and Dusan Odstrcil for their assistance in evaluating this paper.

References

Arge, C. N., D. Odstrcil, V. J. Pizzo, and L. R. Mayer (2003), Improved method for specifying solar wind speed near the Sun, in *Solar Wind Ten*, edited by M. Velli, R. Bruno, and F. Malara, *AIP Conf. Proc.*, *679*, 190.

Arge, C. N., J. G. Luhmann, D. Odstrcil, C. J. Scrijver, and Y. Li (2004), Stream structure and coronal sources of the solar wind during the May 12th, 1997 CME, *J. Atmos. Solar Terr. Phys.*, *66*, 1295.

Burlaga, L. F. (1988), Magnetic clouds: Constant alpha force-free configurations, *J. Geophys. Res.*, *93*, 7217.

Burlaga, L. F., E. Sittler, F. Mariani, and R. Schwenn (1981), Magnetic loop behind and interplanetary shock: Voyager, Helios, and IMP 8 observations, *J. Geophys. Res.*, *86*, 6673.

Burlaga, L. F., et al. (1998), A magnetic cloud containing prominence material: January 1997, *J. Geophys. Res.*, *10*, 277.

Burton, M. E., G. L. Siscoe, and E. J. Smith (1992), Shapes of strong shock fronts propagating through the coronal streamer belt, *J. Geophys. Res.*, *97*, 12,283.

Cane, H. V., and I. G. Richardson (2003), Interplanetary coronal mass ejections in the near-Earth solar wind during 1996–2002, *J. Geophys. Res.*, *108*(A4), 1156, doi:10.1029/2002JA009817.

Cargill, P. J. (2004), On the aerodynamic drag force acting on coronal mass ejections, *Sol. Phys.*, *221*, 135.

Gopalswamy, N. (2004), A global picture of CMEs in the inner heliosphere, in *in The Sun and the Heliosphere As an Integrated System*, *Astrophys.*

and Space Sci. Libr. Ser., edited by G. Poletto and S. Suess, pp. 201–251, Springer, New York.

Hundhausen, A. J. (1993), Sizes and locations of coronal mass ejections: SMM observations from 1980 and 1984–1989, *J. Geophys. Res.*, *98*, 13,177.

Jackson, B. V., P. P. Hick, and A. Buffington (2004a), Time-dependent tomography of heliospheric features using the three-dimensional reconstruction techniques developed for the solar mass ejection imager (SMEI), in *Innovative Telescopes and Instrumentation for Solar Astrophysics*, edited by S. L. Keil and S. V. Avakyan, *Proc. SPIE*, *4853*, 23–30.

Jackson, B. V., et al. (2004b), The Solar Mass-Ejection Imager (SMEI) mission, *Sol. Phys.*, *225*, 177.

Lepping, R. P., et al. (1995), The Wind magnetic-field investigation, *Space Sci. Rev.*, *71*, 207.

Lepping, R. P., et al. (1997), The Wind magnetic cloud and events of October 18–20, 1995: Interplanetary properties and as triggers for geomagnetic activity, *J. Geophys. Res.*, *102*, 14,049.

Linker, J., et al. (1999), Magnetohydrodynamic modeling of the solar corona during Whole Sun Month, *J. Geophys. Res.*, *104*, 9809.

Manchester, W. B., IV, T. I. Gombosi, I. Roussev, A. Ridley, D. L. De Zeeuw, I. V. Sokolov, K. G. Powell, and G. Toth (2004), Modeling a space weather event from the Sun to the Earth: CME generation and interplanetary propagation, *J. Geophys. Res.*, *109*, A02107, doi:10.1029/2003JA010150.

McComas, D. J., H. A. Elliott, N. A. Schwadron, J. T. Gosling, R. M. Skoug, and B. E. Goldstein (2003), The three-dimensional solar wind around solar maximum, *Geophys. Res. Lett.*, *30*(10), 1517, doi:10.1029/2003GL017136.

Michalek, G., N. Gopalswamy, and S. Yashiro (2003), A new method for estimating widths, velocities, and source location of halo coronal mass ejections, *Astrophys. J.*, *584*, 472.

Mulligan, T., and C. T. Russell (2001), Mulitspacecraft modeling of the flux rope structure of interplanetary coronal mass ejections: Cylindrical symmetric versus nonsymmetric topologies, *J. Geophys. Res.*, *106*, 10,581.

Odstrcil, D., and V. J. Pizzo (1999), Three-dimensional propagation of coronal mass ejections (CMEs) in a structured solar wind flow: 1. CME launched within the streamer belt, *J. Geophys. Res.*, *104*, 483.

Odstrcil, D., V. Pizzo, J. A. Linker, P. Riley, R. Lionello, and Z. Mikic (2004a), Initial coupling of coronal and heliospheric numerical magnetohydrodynamic codes, *J. Atmos. Solar Terr. Phys.*, *66*, 1311.

Odstrcil, D., P. Riley, and X. P. Zhao (2004b), Numerical simulation of the 12 May 1997 interplanetary CME event, *J. Geophys. Res.*, *109*, A02116, doi:10.1029/2003JA010135.

Owens, M. J., and P. J. Cargill (2004), Non-radial solar wind flows induced by the motion of interplanetary coronal mass ejections, *Ann. Geophys.*, *22*, 4397.

Owens, M. J., V. G. Merkin, and P. Riley (2006), A kinematically distorted flux rope model for magnetic clouds, *J. Geophys. Res.*, *111*, A03104, doi:10.1029/2005JA011460.

Riley, P., and N. U. Crooker (2004), Kinematic treatment of CME evolution in the solar wind, *Astrophys. J.*, *600*, 1035.

Riley, P., J. T. Gosling, and V. J. Pizzo (1997), A two-dimensional simulation of the radial and latitudinal evolution of a solar wind disturbance driven by a fast, high-pressure coronal mass ejection, *J. Geophys. Res.*, *102*, 14,677.

Riley, P., J. A. Linker, R. Lionello, Z. Mikic, D. Odstrcil, M. A. Hidalgo, Q. Hu, R. P. Lepping, B. J. Lynch, and A. Rees (2004), Fitting flux-ropes to a global MHD solution: A comparison of techniques, *J. Atmos. Solar Terr. Phys.*, *66*, 1321.

Schmidt, J. M., and P. J. Cargill (2001), Magnetic cloud evolution in a two-speed solar wind, *J. Geophys. Res.*, *106*, 8283.

Smith, Z. K., D. Odstrcil, M. Vandas, S. Fischer, P. Pelant, and M. Dryer (1996), The role of magnetic fields and the heliospheric current sheet in the interplanetary evolution of disturbances caused by solar drivers, in *Solar Drivers of the Interplanetary and Terrestrial Disturbances*, *Astron. Soc. of the Pac. Conf. Ser.*, vol. 16, edited by K. S. Balasubramaniam, S. L. Keil, and R. N. Smartt, p. 341, Astron. Soc. of the Pac., San Fransisco, Calif.

St Cyr., O. C., et al. (2000), Properties of coronal mass ejections: SOHO LASCO observations from January 1996 to June 1998, *J. Geophys. Res.*, *105*, 18,169.

Webb, D. F., R. P. Lepping, L. F. Burlaga, C. E. DeForest, D. E. Larson, S. F. Martin, S. P. Plunkett, and D. M. Rust (2000), The origin and development of the May 1997 magnetic cloud, *J. Geophys. Res.*, *105*, 27,251.

Zhao, X. P., S. P. Plunkett, and W. Liu (2002), Determination of geometrical and kinematical properties of halo coronal mass ejections using the cone model, *J. Geophys. Res.*, *107*(A8), 1223, doi:10.1029/2001JA009143.

M. J. Owens, Center for Space Physics, Boston University, Boston, MA 02215, USA. (mjowens@bu.edu)